Beam coupling impedances for perforated beam pipes with general shape from impedance boundary conditions

Stefania Petracca
University of Sannio at Benevento and INFN, Salerno, Italy
(Received 5 October 1998; revised manuscript received 20 May 1999)

An equivalent wall impedance to describe the electromagnetic boundary conditions at perforated pipe walls is introduced. The new impedance boundary condition, together with general formulas for computing longitudinal and transverse beam coupling impedances in complex heterogeneous pipes, provides a good trade-off between computational accuracy and ease. [S1063-651X(99)11209-1]

PACS number(s): 03.50.De, 41.20.Cv

I. INTRODUCTION

In the foreseen large hadron collider (LHC) design [1], the stainless-steel vacuum chamber (cold bore) will be kept at 1.9 K using superfluid helium, and protected from synchrotron radiation by a beam screen cooled at some 4.5–20 K. Gas desorption due to synchrotron radiation, and subsequent surface deposition, limits the pumping efficiency of the beam pipe vacuum system, unless many holes or slots are drilled in the beam screen wall, allowing for a transfer of the excess gas to the 1.9-K cold bore, where the pumping capacity is adequate. At the present stage of the project, the total number of holes or slots should be as large as $10^7 - 10^8$ ($10^2 - 10^3$ holes/slots per meter), with typical sizes of ~ 2 mm diam (holes) or 1.5×8mm (slots). The effect of so many holes/slots on the beam dynamics and stability, e.g., in terms of coupling impedances, is a fundamental issue and has been carefully investigated, both theoretically [2–7], and experimentally [8,9].

In this paper we introduce a (local) impedance boundary condition of the Leontóvich type [10], to describe *perforated* pipe walls [11]. The latter can be used within the general framework presented in [12] and summarized in Sec. II to obtain analytic estimates, based on reciprocity formulas, of the longitudinal and transverse coupling impedances for *heterogeneous* beam pipes with *complex* geometry, including (partially) perforated walls. The rest of the paper is accordingly organized as follows.

In Sec. III we introduce an impedance boundary condition appropriate to a thin perfectly conducting pipe wall with many (noninteracting) electrically *small* holes in free space following a *heuristic* argument. In Sec. IV we derive the same result by solving a rigorous boundary value problem. Possible model improvements are considered in Sec. V, including (i) holes in a thick wall, (ii) interacting holes, and (iii) perforated beam pipes in a coaxial lossy tube. In Sec. VI we apply the above to the computation of perforated wall impedances at fixed pumping capacity, for a proposed LHC pipe geometry. In Sec. VII we compute the related parasitic losses (both Ohmic and due to leakage through the holes). Conclusions follow under Sec. VIII. Relevant tools and definitions are collected in Appendixes A–C.

II. COUPLING IMPEDANCES IN COMPLEX PIPES

A simple and fairly accurate relationship between the specific longitudinal and transverse beam coupling impedances $Z_{0,\|}(\omega)$ and $\bar{\bar{Z}}_{0,\perp}(\omega)$ of a *simple*, *unperturbed* pipe (e.g., circular, perfectly conducting) assumed known, and those $Z_{\|}(\omega)$, $\bar{\bar{Z}}_{\perp}(\omega)$ of another pipe differing from the former by some *perturbation* in the boundary geometry and/or constitutive properties, were obtained in [12], by using the electromagnetic reciprocity principle, viz.,

$$Z_{\|}(\omega) - Z_{0,\|}(\omega) = \frac{\epsilon_0}{\beta_0 c Q^2} \left\{ Y_0 \oint_{\partial S} Z_{\rm wall} E_{0n}^{(\rm irr)} *(\vec{r},0) \times [\beta_0 E_n^{(\rm irr)}(\vec{r},0) + \beta_0^{-1} E_n^{(\rm sol)}(\vec{r},0)] d\ell - \oint_{\partial S} E_{0z}^{*}(\vec{r},0) E_n^{(\rm irr)}(\vec{r},0) d\ell \right\}, \tag{1}$$

$$\bar{\bar{Z}}_{\perp}(\omega) - \bar{\bar{Z}}_{0,\perp}(\omega) = \frac{\epsilon_0}{\beta_0 c Q^2 k} \left\{ Y_0 \oint_{\partial S} Z_{\rm wall} \vec{\nabla}_{\vec{r}_0} E_{0n}^{(\rm irr)} *(\vec{r},\vec{r}_0) \otimes \vec{\nabla}_{\vec{r}_1} [\beta_0 E_n^{(\rm irr)}(\vec{r},\vec{r}_1) + \beta_0^{-1} E_n^{(\rm sol)}(\vec{r},\vec{r}_1)] d\ell - \oint_{\partial S} \vec{\nabla}_{\vec{r}_0} E_{0z}^{*}(\vec{r},\vec{r}_0) \otimes \vec{\nabla}_{\vec{r}_1} E_n^{(\rm irr)}(\vec{r},1) d\ell \right\}_{\vec{r}_1 = \vec{r}_0 = 0}, \tag{2}$$

where $c = (\epsilon_0 \mu_0)^{-1/2}$ is the speed of light in vacuum, $Y_0 = (\epsilon_0/\mu_0)^{1/2}$ is the vacuum characteristic admittance, ϵ_0 and μ_0 being the vacuum permittivity and permeability, β_0 is the relativistic factor, Q is the total beam charge [13], $\vec{E}_0^{(\rm sol)}, \vec{E}_0^{(\rm irr)}$ are the solenoidal and irrotational parts of the electric field in the *unperturbed* pipe, the unit vectors $\hat{u}_c, \hat{u}_n, \hat{u}_z$ are defined in Fig. 1, $\bar{\bar{Z}}_{\perp}(\omega)$ is a tensor, and one assumes an impedance (Leontóvich) boundary condition to hold at the pipe wall ∂S:

$$|(\bar{\bar{I}} - \hat{u}_n \hat{u}_n) \cdot \vec{E} - Z_{\rm wall} \hat{u}_n \times \vec{H}|_{\partial S} = 0, \tag{3}$$

where $Z_{\rm wall}$ is the pipe-wall complex characteristic impedance.

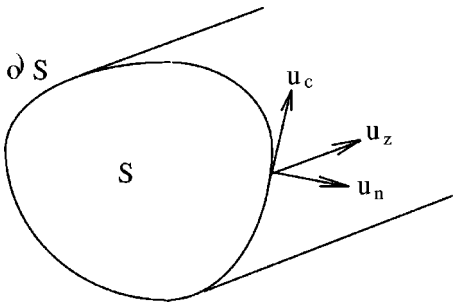

FIG. 1. The unit vectors $\hat{u}_c, \hat{u}_n, \hat{u}_z$ relevant to Eqs. (1) and (2).

The first integral term on the right-hand side of Eq. (1) accounts for the effect of the finite wall conductivity, and is nonzero if and only if $Z_{\rm wall}$ is not identically zero on ∂S. The second integral on the right-hand side of Eq. (1), on the other hand, accounts for the effect of the geometrical perturbation of the boundary, and is nonzero if and only if the *unperturbed* axial field component E_{0z} is not identically zero on ∂S [13].

For the simplest case of a circular pipe with radius b and uniform wall impedance $Z_{\rm wall}$, one readily obtains from Eq. (1)

$$Z_{\parallel}=\frac{Z_{\rm wall}}{2\pi b}, \quad \bar{\bar{Z}}_{\perp}=\frac{Z_{\rm wall}}{\pi k_0 b^3}(\hat{u}_x\hat{u}_x+\hat{u}_y\hat{u}_y), \tag{4}$$

in agreement with the known exact result [14].

III. IMPEDANCE BOUNDARY CONDITIONS AT PERFORATED BEAM PIPE WALLS: HEURISTICS

Extensive calculations and estimates for the longitudinal and transverse impedances per unit length in perforated beam pipes have been presented by Kurennoy [15] and Gluckstern [2–5].

According to these authors, the longitudinal impedance per unit length of a circular beam pipe with radius b carrying N_λ holes per unit length is [17]

$$Z_{\parallel}=-jZ_0k_0\frac{(\alpha_e+\alpha_m)}{4\pi^2b^2}N_\lambda, \tag{5}$$

where $k_0=\omega/c$ is the free-space wave number and $\alpha_{e,m}$ are the electric and magnetic polarizabilities [18] of each hole [19]. The result (5) does not depend on the azimuthal position of the holes, such being the field produced by an axial beam in a circular pipe. Thus, letting

$$n_\sigma=\frac{N_\lambda}{2\pi b} \tag{6}$$

represent the number of holes per unit wall area, Eq. (5) can be written as

$$Z_{\parallel}=-jZ_0k_0\frac{(\alpha_e+\alpha_m)}{2\pi b}n_\sigma. \tag{7}$$

By comparing Eqs. (7) and (4), one is led to the heuristic conclusion that a perforated wall could be described by an impedance boundary condition with

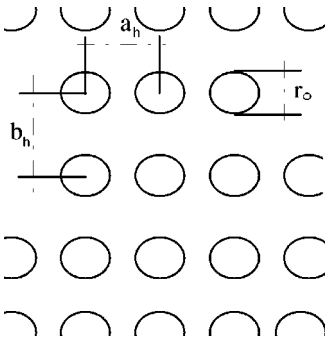

FIG. 2. Regular 2D array of circular holes on a conducting plane $z=0$.

$$Z_{\rm wall}=-jZ_0k_0(\alpha_e+\alpha_m)n_\sigma. \tag{8}$$

Using Eq. (8) in Eqs. (1) and (2) would allow us to estimate the longitudinal and transverse beam impedances under very general assumptions, including, e.g., pipes with *unevenly* distributed holes and complicated transverse geometries. This is indeed the case [23], as can be seen by considering a pipe with *general* transverse geometry carrying N_λ (uniformly spaced) holes per unit length, located at $\ell=\ell_h$, ℓ being the arc length along the pipe cross-section contour ∂S, for which

$$n_\sigma=N_\lambda\delta(\ell-\ell_h). \tag{9}$$

Using Eq. (9) in Eq. (1) gives

$$Z_{\parallel}=-jZ_0k_0(\alpha_e+\alpha_m)e_n(\ell_h)e_n^*(\ell_h), \tag{10}$$

where $e_n(\ell_h)=(Q/\epsilon_0)^{-1}E_n(\ell_h)$, $E_n(\ell_h)$ being the normal electric field at the hole position produced by an axial beam with total charge Q. Equation (10) reproduces exactly Kurennoy's result valid for this most general case [2,24].

In the next section we shall further support the heuristic result (8) by solving a rigorous electromagnetic (henceforth EM) boundary value problem.

IV. IMPEDANCE BOUNDARY CONDITIONS AT PERFORATED BEAM PIPE WALLS: BOUNDARY VALUE APPROACH

In this section we consider a (TM) plane wave $(\vec{E}^{(i)},\vec{H}^{(i)})$:

$$\vec{k}^{(i)}=k_0(\sin\theta\hat{u}_x+\cos\theta\hat{u}_z),$$

$$\vec{H}^{(i)}=H_0\hat{u}_y e^{j\vec{k}^{(i)}\cdot\vec{r}}=H_0\hat{u}_y e^{-jk_0(z\cos\theta+x\sin\theta)}, \tag{11}$$

$$\vec{E}^{(i)}=Z_0\vec{H}^{(i)}\times\vec{k}^{(i)}=(-\sin\theta\hat{u}_z+\cos\theta\hat{u}_x)Z_0H_0e^{j\vec{k}^{(i)}\cdot\vec{r}},$$

incident with an angle θ on a perfectly conducting plane at $z=0$ bearing a regular array of holes at $x=na_h$, $y=mb_h$, $m,n=-\infty,\ldots,\infty$ (see Fig. 2). In Eq. (11), $Z_0=(\mu_0/\epsilon_0)^{1/2}$ is the free-space impedance. Note that we use the $\exp(-j\omega t)$ time dependence to comply with the particle accelerator literature.

In the limit of near-grazing incidence $\theta\to\pi/2$, the primary field (holes suppressed) has the same local structure at $z=0$ as the field of a relativistic particle beam at a perfectly

conducting pipe wall: the magnetic field is nearly tangent to the wall, and the electric field nearly normal. Thus, following [25], we expect to be able to deduce an appropriate (local) impedance boundary condition from the asymptotic ($\theta \to \pi/2$) form of the TM plane-wave reflection coefficient.

If the holes were absent the reflected field $(\vec{E}^{(r)},\vec{H}^{(r)})$ would be

$$\vec{k}^{(r)} = k_0(\sin\theta\,\hat{u}_x - \cos\theta\hat{u}_z),$$

$$\vec{H}^{(r)} = H_0\hat{u}_y e^{j\vec{k}^{(r)}\cdot\vec{r}} = H_0\hat{u}_y e^{jk_0(-z\cos\theta + x\sin\theta)}, \tag{12}$$

$$\vec{E}^{(r)} = Z_0\vec{H}^{(r)}\times\vec{k}^{(r)} = (-\sin\theta\hat{u}_z - \cos\theta\hat{u}_x)Z_0H_0e^{j\vec{k}^{(r)}\cdot\vec{r}},$$

and the total field would be

$$(\vec{E}_{\rm tot},\vec{H}_{\rm tot}) = \begin{cases} 0, & z>0, \\ (\vec{E}^{(i)}+\vec{E}^{(r)},\vec{H}^{(i)}+\vec{H}^{(r)}), & z<0. \end{cases} \tag{13}$$

The field in the presence of the holes, according to Bethe's approximation [18], can be computed by *adding* to the primary field (13) above, the field $\vec{E}^{(\rm scatt)}$, $\vec{H}^{(\rm scatt)}$ produced by elementary electric and magnetic sources radiating on a perfectly conducting (no hole) plane $z=0$ and placed at $x = na_h$, $y = mb_h$, $m,n = -\infty,\ldots,\infty$.

Specifically, the sources at $\vec{r} = \vec{r}_{nm} = na_h\hat{u}_x + mb_h\hat{u}_y$ have moment densities:

$$\vec{P}_{nm} = \epsilon_0\alpha_e\delta(\vec{r}-\vec{r}_{mn})E_z^{(\rm tot)}(\vec{r}_{mn})\hat{u}_z,$$
$$\vec{M}_{nm} = \alpha_m\delta(\vec{r}-\vec{r}_{mn})(\bar{\bar{I}}-\hat{u}_z\hat{u}_z)\vec{H}^{(\rm tot)}(\vec{r}_{mn}), \tag{14}$$

where α_e and α_m are the hole electric and magnetic polarizabilities [26].

It is seen from Eqs. (13), (11), and (12) that

$$E_z^{(\rm tot)}(z=0) = 2E_z^{(i)}(z=0) = -Z_0H_0\sin\theta e^{jk_0x\sin\theta}, \tag{15}$$

$$(\bar{\bar{I}}-\hat{u}_z\hat{u}_z)\cdot\vec{H}^{(\rm tot)}(z=0) = (\bar{\bar{I}}-\hat{u}_z\hat{u}_z)\cdot 2\vec{H}^{(i)}(z=0) = 2H_0\hat{u}_y e^{jk_0x\sin\theta}.$$

Furthermore, the fields radiated in $z<0$ by the dipoles (14) sitting on the perfectly conducting plane $z=0$ are the same as those radiated *in free space* by Eqs. (14) and their images [27]. The images are equiverse and placed exactly at the same positions as the corresponding primary sources. Thus the superposition of the primary and image sources is just *twice* Eqs. (14), viz.,

$$\vec{P}_{\rm tot} = \sum_{m,n}(\vec{P}_{m,n}+\vec{P}^{(\rm image)}_{m,n}) = \sum_{m,n}2\vec{P}_{m,n}$$
$$= -4c^{-1}H_0\alpha_e\sin\theta\delta(z)\sum_{m,n}\delta(x-na_h)\times\delta(y-mb_h)e^{jk_0na_h\sin\theta}\hat{u}_z, \tag{16}$$

$$\vec{M}_{\rm tot} = \sum_{m,n}(\vec{M}_{m,n}+\vec{M}^{(\rm image)}_{m,n}) = \sum_{m,n}2\vec{M}_{m,n}$$
$$= 4H_0\alpha_m\delta(z)\sum_{m,n}\delta(x-na_h)\,\delta(y-mb_h)e^{jk_0na_h\sin\theta}\hat{u}_y. \tag{17}$$

The fields produced by these sources can be quickly computed using the vector potential $\vec{A}$ and the magnetic Hertz potential $\vec{\Pi}$, which are related to $\vec{P}_{\rm tot}$ and $\vec{M}_{\rm tot}$ by

$$(\nabla^2+k_0^2)\vec{A} = j\omega\mu_0\vec{P}_{\rm tot},$$
$$(\nabla^2+k_0^2)\vec{\Pi} = -\vec{M}_{\rm tot}, \tag{18}$$

as follows:

$$\vec{E}^{(\rm scatt)} = -j\omega c^{-2}\vec{\nabla}\times\vec{\nabla}\times\vec{A} + j\omega\mu_0\vec{\nabla}\times\vec{\Pi},$$
$$\vec{H}^{(\rm scatt)} = \mu_0^{-1}\vec{\nabla}\times\vec{A} + \vec{\nabla}\times\vec{\nabla}\times\vec{\Pi}. \tag{19}$$

In order to solve Eqs. (18) it is first expedient to note that since $\vec{P}_{\rm tot} = P\hat{u}_z$ and $\vec{M}_{\rm tot} = M\hat{u}_y$, then $\vec{A} = A\hat{u}_z$ and $\vec{\Pi} = \Pi\hat{u}_y$. It is further convenient to use the (generalized) Fourier representation of the periodic δ functions:

$$\sum_n^{-\infty,\infty}\delta(x-na_h) = \frac{1}{a_h}\sum_p^{-\infty,\infty}e^{jq(2\pi/a_h)x}, \tag{20}$$

$$\sum_m^{-\infty,\infty}\delta(y-mb_h) = \frac{1}{a_h}\sum_q^{-\infty,\infty}e^{jq(2\pi/b_h)y}, \tag{21}$$

so as to recast the source terms into the following form:

$$\vec{P}_{\rm tot} = -\frac{4H_0\alpha_e}{cb_ha_h}\sin\theta\delta(z)\sum_{p,q}^{-\infty,\infty}e^{2\pi j(px/a_h+qy/b_h)}e^{jk_0x\sin\theta}\hat{u}_z, \tag{22}$$

$$\vec{M}_{\rm tot} = \frac{4H_0\alpha_m}{b_ha_h}\delta(z)\sum_{p,q}^{-\infty,\infty}e^{2\pi j(px/a_h+qy/b_h)}e^{jk_0x\sin\theta}\hat{u}_y,$$

and obtaining the following wave equations:

$$(\nabla^2+k_0^2)A = -j\omega\mu_0\frac{4H_0\alpha_e}{ca_hb_h}\sin\theta\,\delta(z)\times\sum_{p,q}^{-\infty,\infty}e^{2\pi j(px/a_h+qy/b_h)}e^{jk_0x\sin\theta}, \tag{23}$$

$$(\nabla^2+k_0^2)\Pi = -\frac{4H_0\alpha_m}{a_hb_h}\delta(z)\sum_{p,q}^{-\infty,\infty}e^{2\pi j(px/a+qy/b)}e^{jk_0x\sin\theta}.$$

The forcing terms in Eqs. (23) contain δ functions at $z=0$, and thus the equations must be solved in the weak (Sobolev) sense.

The form of the equations suggests that the solutions have the same x,y dependence as the corresponding forcing terms, and thus can be written as

$$A=\sum_{p,q}^{-\infty,\infty} A_{p,q}e^{\pm j\gamma_{p,q}z}e^{j[k_0x\sin\theta+2\pi(px/a_h+qy/b_h)]},\quad z\gtrless 0, \tag{24}$$

$$\Pi=\sum_{p,q}^{-\infty,\infty} \Pi_{p,q}e^{\pm j\eta_{p,q}z}e^{j[k_0x\sin\theta+2\pi(px/a_h+qy/b_h)]},\quad z\gtrless 0,$$

where $\gamma_{p,q}$ and $\eta_{p,q}$ are non-negative defined, and the choice of the sign in the z-dependent exponentials corresponds to the physical requirement that the waves produced by the sources (22) propagate *away* from the plane where they lie ($z=0$).

Setting Eq. (24) into Eq. (23), for $z\neq 0$, one readily gets

$$\gamma_{p,q}=\eta_{p,q}=+\sqrt{k_0^2-\left\{\left(\frac{2\pi q}{b_h}\right)^2+\left[\left(\frac{2\pi p}{a_h}\right)+k_0\sin\theta\right]^2\right\}}. \tag{25}$$

Each term in Eqs. (24) is recognized to represent a plane wave propagating in the (p,q) *grating lobe* direction, with wave vector

$$k_x=\frac{2\pi}{a_h}p+k_0\sin\theta,\quad k_y=\frac{2\pi}{b_h}q,\quad k_z=\pm[k_0^2-(k_x^2+k_y^2)]^{1/2} \tag{26}$$

for $z\gtrless 0$. In particular, the $p=q=0$ term propagates, for $x<0$, in the specular reflection direction [28], with wave vector

$$k_x=k_0\sin\theta,\quad k_y=0,\quad k_z=-k_0\cos\theta. \tag{27}$$

In order to determine the coefficients $A_{p,q}$ and $\Pi_{p,q}$, we require that Eqs. (24) be weak solutions of Eqs. (23), by integrating them across $z=0$, viz.,

$$\begin{aligned} j\omega\mu_0\int_{0-}^{0+}dz\,P_{\rm tot}&=\int_{0-}^{0+}dz(\nabla^2+k_0^2)A\\ &=\int_{0-}^{0+}dz(\partial_{xx}^2+\partial_{yy}^2+k_0^2)A+\left|\partial_zA\right|_{z=0-}^{z=0+}, \end{aligned} \tag{28}$$

and the like for Π. The first term on the right-hand side of Eq. (28) is zero, because the integrand is continuous and limited across $z=0$. The second is nonzero, because ∂_zA is *discontinuous* across $z=0$, due to the *different* signs of the z-dependent exponential for $z>0$ and $z<0$ in Eqs. (24). Hence, using Eqs. (22) and (24) in Eq. (28) one gets

$$A_{p,q}=2\frac{k_0H_0}{a_hb_h\gamma_{p,q}}\sin\theta\mu_0\alpha_e, \tag{29}$$

$$\Pi_{p,q}=-j\frac{2H_0}{a_hb_h\eta_{p,q}}\alpha_m. \tag{30}$$

The reflection coefficient of the perforated wall can now be defined with reference to the *specular* component ($p=q=0$) of the scattered field [29]:

$$\Gamma_H=\left.\frac{H_{0,0}^{(\rm scatt)}+H^{(r)}}{H^{(i)}}\right|_{z=0}:=-\frac{Z_{z>0}-Z_{z<0}}{Z_{z>0}+Z_{z<0}}, \tag{31}$$

where the last equality defines the reflection coefficient at $z=0$ in terms of the *oblique* wave impedances [30] $Z_{z<0}$ and $Z_{z>0}$ of the *media* filling the $z<0$ and $z>0$ half-spaces.

The scattered magnetic field can be easily computed using Eqs. (19), (24), (29), and (30). One readily obtains [31]

$$H_{0,0}^{(\rm scatt)}=2jk_0\frac{\alpha_m+\alpha_e\sin^2\theta}{a_hb_h\cos\theta}H_0e^{j\vec{k}^{(r)}\cdot\vec{r}} \tag{32}$$

and hence, substituting into Eq. (31),

$$\Gamma_H=1+2jk_0\frac{\alpha_m+\alpha_e\sin^2\theta}{a_hb_h\cos\theta}\approx 1-2\frac{Z_{z>0}}{Z_{z<0}}=1-2\frac{Z_{z>0}}{Z_0\cos\theta}, \tag{33}$$

where the fraction on the right-hand side of Eq. (31) has been expanded to lowest order [32] in the ratio $Z_{z>0}/Z_{z<0}$. Hence

$$Z_{z>0}=-j\frac{k_0Z_0}{a_hb_h}(\alpha_m+\alpha_e\sin^2\theta). \tag{34}$$

We are thus led to conclude that, for *close-to-grazing* incident fields, a perforated perfectly conducting wall acts like the surface of a homogeneous medium with (oblique) wave impedance

$$Z_{z>0}=-j\frac{k_0Z_0}{a_hb_h}(\alpha_m+\alpha_e). \tag{35}$$

Note that the spatial distribution of the holes appears in Eq. (35) only through the factor $(a_hb_h)^{-1}$, which represents the number of holes per unit area n_σ. Hence

$$Z_{z>0}=-jk_0Z_0(\alpha_m+\alpha_e)n_\sigma, \tag{36}$$

which reproduces our heuristic ansatz (8).

As a matter of fact, the impedance (36) is usually *very small*, and thus provided the further condition (see Appendix A)

$$\left|\left(\frac{Z_0}{Z_{z>0}}\right)k_0\rho_S\right|\gg 1 \tag{37}$$

is satisfied, ρ_S being the (local) smallest radius of curvature of the surface S, then a Leontóvich boundary condition (3) with $Z_{\rm wall}$ given by Eq. (36) can be used even for a *nonplanar*, perfectly conducting, perforated surface.

This provides a rigorous justification of our heuristic ansatz (8). In the following we shall denote the wall impedance of a perforated pipe wall in free space by $Z_{p.w.}^{(0)}$.

V. POSSIBLE MODEL IMPROVEMENTS

It is conceivable and relatively straightforward to improve the model by, e.g, (i) including the effect of a nonzero wall thickness; (ii) describing the effect of electromagnetic coupling among the holes; (iii) taking into account the presence of a further (imperfectly conducting) tube surrounding the perforated beam pipe.

Note that all *potential* improvements of Eq. (36) should be gauged consistently against the omission of terms of higher order in $k\times$(hole size) in the standard (Bethe's) formulas for $\alpha_{e,m}$. These terms have been discussed in [33–35].

In this section we shall briefly review points (i)–(iii) above.

A. Holes in a thick wall

A nonzero wall thickness is useful to reduce radiation leakage through the pumping holes. A general formalism for computing electric and magnetic hole polarizabilities for thick walls has been set up in [36–38]. For circular holes one has, with good accuracy [39]:

$$(\alpha_e^{(i)}+\alpha_m^{(i)})\approx 0.57(\alpha_e^{(0)}+\alpha_m^{(0)}), \quad w/r_0\leqslant 2, \tag{38}$$

$$\alpha_e^{(e)}=\frac{2}{3}r_0^3\exp(-\xi_{\mathrm{TE}}w/r_0), \tag{39}$$

$$\alpha_m^{(e)}=-\frac{4}{3}r_0^3\exp(-\xi_{\mathrm{TM}}w/r_0), \tag{40}$$

where the superscripts (i), (e), and (0) identify the internal, external, and thin-wall polarizabilities, r_0 is the hole radius and w the wall thickness, and $\xi_{\mathrm{TE}}=2.405$ and $\xi_{\mathrm{TM}}=1.841$ are the damping constants of the dominant transverse-electric (TE) and transverse-magnetic (TM) cutoff modes of a circular waveguide having the same radius as the holes.

B. Coupling among holes

Electromagnetic coupling among the holes can be accounted for by using in Eq. (36) the *effective* electric polarizabilities $\alpha'_{e,m}$ of each hole, *in the presence of the others*, viz.,

$$\alpha'_{e,m}=\frac{\alpha_{e,m}}{1-C_{e,m}\alpha_{e,m}}, \tag{41}$$

where the coupling constants $C_{e,m}$ are given in Appendix B. For a relativistic beam, the induced *electric* dipoles are *normal* to the perforated wall, while the *magnetic* ones are *tangent* and, for circular holes, *parallel* to the magnetic field. Thus, Eqs. (B5)–(B7), under the further assumption $a=b=s$, specialize to

$$C_e=C_\perp=s^{-3}\left[-\frac{12}{5\pi}+16\pi K_0(2\pi)\right], \tag{42}$$

$$C_m=C_\parallel=s^{-3}\left[\frac{6}{5\pi}-8\pi K_0(2\pi)\right], \tag{43}$$

where K_0 is a zeroth-order modified Bessel function of the second kind. Equations (42) and (43) imply a quasistatic ($s\ll\lambda$) assumption, which could be removed in principle [40].

C. Perforated beam pipe in a coaxial lossy tube

The influence of an external imperfectly conducting tube (e.g., a cold bore), coaxial to the beam pipe can be simply described by using *modified* polarizabilities in Eqs. (7) and (8). The modified polarizabilities have the simple form [41–43]

$$\alpha'_{e,m}=\alpha_{e,m}^{(i)}+F\alpha_{e,m}^{(e)}, \tag{44}$$

where for a circular liner in a coaxial circular cold bore [44],

$$F=-\frac{\alpha_e^{(e)}+\alpha_m^{(e)}}{\alpha_e^{(i)}+\alpha_m^{(i)}+j\,\mathrm{sgn}(k)\,\hat{\delta}^*n_\sigma^{-1}(1+b/a)}, \tag{45}$$

or, equivalently,

$$F=-\frac{(\alpha_e^{(e)}+\alpha_m^{(e)})(\alpha_e^{(i)}+\alpha_m^{(i)})^{-1}}{1+\dfrac{(1+b/a)Z_{\mathrm{cb}}}{Z_{\mathrm{p.w.}}^{(0)}}}. \tag{46}$$

In Eqs. (44), (45), and (46) the superscripts (e) and (i) denote the external and internal polarizabilities, $\hat{\delta}=(|k_0|Z_0)^{-1}\ Z_{\mathrm{cb}}^*$ is the *complex* EM penetration depth into the cold-bore walls (both walls at $r=b+$ and $r=a$ assumed lossy, with finite conductivity σ_{cb}), and Z_{cb} the corresponding (complex) wall impedance:

$$Z_{\mathrm{cb}}=[1-j\,\mathrm{sgn}(\omega)]\left(\frac{|k_0|Z_0}{2\sigma_{\mathrm{cb}}}\right)^{1/2}. \tag{47}$$

Hence, Eqs. (7) and (8) become

$$Z_\parallel=-j\frac{Z_0k_0n_\sigma}{2\pi b}\left[(\alpha_e^{(i)}+\alpha_m^{(i)})-\frac{(\alpha_e^{(e)}+\alpha_m^{(e)})^2(\alpha_e^{(i)}+\alpha_m^{(i)})^{-1}}{1+\dfrac{(1+b/a)Z_{\mathrm{cb}}}{Z_{\mathrm{p.w.}}^{(0)}}}\right], \tag{48}$$

$$Z_{\mathrm{wall}}=-jZ_0k_0n_\sigma\left[(\alpha_e^{(i)}+\alpha_m^{(i)})-\frac{(\alpha_e^{(e)}+\alpha_m^{(e)})^2(\alpha_e^{(i)}+\alpha_m^{(i)})^{-1}}{1+\dfrac{(1+b/a)Z_{\mathrm{cb}}}{Z_{\mathrm{p.w.}}^{(0)}}}\right]. \tag{49}$$

In the limit of an infinitely thin liner's wall, where $\alpha_{e,m}^{(e)}=-\alpha_{e,m}^{(i)}$, Eq. (49) admits a simple physical interpretation.

The complex propagation constant and characteristic impedance of the lossy coaxial cold-bore waveguide can be equivalently computed by assuming that the inner ($r=a-$) cold-bore wall is a *perfect conductor* (as assumed in [43]) and placing an *equivalent* wall impedance:

$$Z_{\mathrm{eq}}=Z_{\mathrm{cb}}\left(1+\frac{b}{a}\right) \tag{50}$$

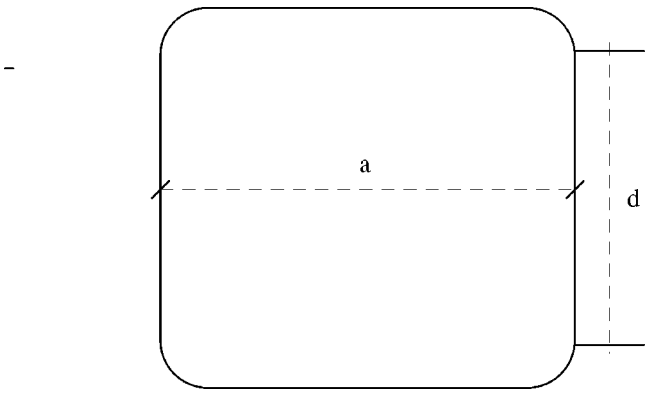

FIG. 3. Rounded corner square liner cross section.

on the outer liner wall ($r=b+$) alone [45]. Then, it is readily seen that Eq. (49) is nothing but the parallel combination of $Z^{(0)}_{\text{p.w.}}$ given by Eq. (8) and Z_{eq} (50),

$$Z_{\text{wall}}=\frac{Z^{(0)}_{\text{p.w.}}Z_{\text{eq}}}{Z^{(0)}_{\text{p.w.}}+Z_{\text{eq}}}. \tag{51}$$

The power lost in the coaxial waveguide between the liner and the cold bore has been predicted and measured in [8,9], and confirms the validity of the above analysis [46].

VI. PERFORATED WALL IMPEDANCES AT FIXED PUMPING CAPACITY

In this section we shall refer to the pipe geometry depicted in Fig. 3: a rounded corner cross-section stainless-steel pipe copper-plated on its straight sides, which has been proposed for LHC [1].

We shall assume that the holes are confined within the rounded corners of the beam pipe contours, where the leaking fields would be at a minimum.

The size of the holes is determined by the requirement of preventing excessive radiation loss through them, while their number is dictated by requiring an adequate pumping capacity. Typical numbers are accordingly shown in Table I.

Each rounded corner has a surface $(\pi/4)(a-d)$ per unit length of liner, thus there are $4(\pi/4)(a-d)n_\sigma$ holes per unit length of liner. Hence, for a regular two-dimensional (2D) lattice of circular holes with spacing s, one has [47]

$$n_\sigma=s^{-2}\frac{N_\lambda}{4a}\left[\frac{\pi}{4}\left(1-\frac{d}{a}\right)\right]^{-1}. \tag{52}$$

TABLE I. Model parameters relevant to Fig. 3.

Stainless-steel resistivity ρ_{ss}	5×10^{-7} Ω m
Copper plating resistivity ρ_{Cu}	5.5×10^{-10} Ω m
Number of particles per bunch	10^{11}
Number of bunches N_b	2835
Revolution frequency ν_r	11.245 kHz
Hole radius r_0	0.75 mm
Wall thickness	0.75 mm
Liner diameter a	3.48 cm
Bunch length σ_z	7.5 cm

As a result, the coupling coefficients (42) and (43) and hence the wall impedance become functions of d/a, as shown in Figs. 4(a)–4(d) and 5(a)–5(d) for several values of the ratio ω/ω_c, $\omega_c=(\pi c/a)$ being the (lowest) pipe cutoff angular frequency [48]. To draw these figures we used the parameters collected in Table I, taking into account wall thickness via Eq. (38), and the presence of the cold-bore via Eqs. (44) and (45).

In Figs. 4(a) and 4(b) the wall resistance and reactance for a thick liner surrounded by a (circular) coaxial cold bore are shown. Those of the same liner in free space are shown in Figs. 4(c) and 4(d) While the effect of the cold bore is quite visible, it is seen that for thick liners including or neglecting hole coupling does not make any sensible difference.

In Figs. 5(a) and 5(b) the wall resistance and reactance for a thin (zero thickness) wall liner are displayed. Those of the same liner in free space are shown in Figs. 5(c) and 5(d). Here we used Kurennoy's result [3]:

$$\left|\frac{\text{Re}[Z_{\text{wall}}]}{\text{Im}[Z_{\text{wall}}]}\right|=\frac{\pi^2}{6}\,\frac{\alpha_e^2+\alpha_m^2}{\alpha_e+\alpha_m}\left(\frac{\omega}{\omega_c}\right)^3 a^{-3} \tag{53}$$

in Eq. (8) together with Eqs. (41) and (43). As for the thick liner, the effect of the cold bore is quite evident, while hole coupling becomes visible as f approaches f_c.

By comparing Figs. 4 and 5, it is seen that the effect of wall thickness cannot be neglected.

VII. PARASITIC LOSSES

The parasitic loss (energy lost by the beam per unit pipe length), is given by [14]

$$\frac{\Delta\mathcal{E}}{L}=\frac{1}{2\pi}\int_{-\infty}^{+\infty}|I(\omega)|^2\,\text{Re}\,Z_\parallel(\omega)\,d\omega, \tag{54}$$

where $I(\omega)$ is the beam current frequency spectrum and $Z_\parallel(\omega)$ is the longitudinal impedance.

In the following we shall again refer to the stainless-steel rounded-corner square cross-section beam-pipe with copper-plated side walls, sketched in Fig. 3 and described in Table I.

For Gaussian bunches of rms length σ_z and total charge Q, the current frequency spectrum is

$$I(\omega)=Qe^{-\sigma_z^2k^2/2}. \tag{55}$$

A. Ohmic losses

The *pure* Ohmic power losses $P^{(0)}_{\text{Cu}}+P^{(0)}_{\text{ss}}$ in the *unperforated* copper-plated and stainless-steel (internal) beam-pipe surfaces, can be written [49]

$$P^{(0)}_{\text{Cu,ss}}=N_b\nu_r\frac{\Delta\mathcal{E}}{L}=N_b\nu_r\frac{Q^2cZ_0}{8\pi^3a^2}W^{(0)}_{\text{Cu,ss}}\left(\frac{\sigma_z}{a}\right)G_{\text{Cu,ss}}\left(\frac{d}{a}\right), \tag{56}$$

where N_b is the number of bunches in the ring, ν_r the revolution frequency, a the (rounded) square side length, Q the bunch charge, the functions $G_{\text{Cu}}(\,)$, $G_{\text{ss}}(\,)$ are defined in Appendix C, and the functions $W^{(0)}_{\text{ss}}(\,)$ and $W^{(0)}_{\text{Cu}}(\,)$ depend only

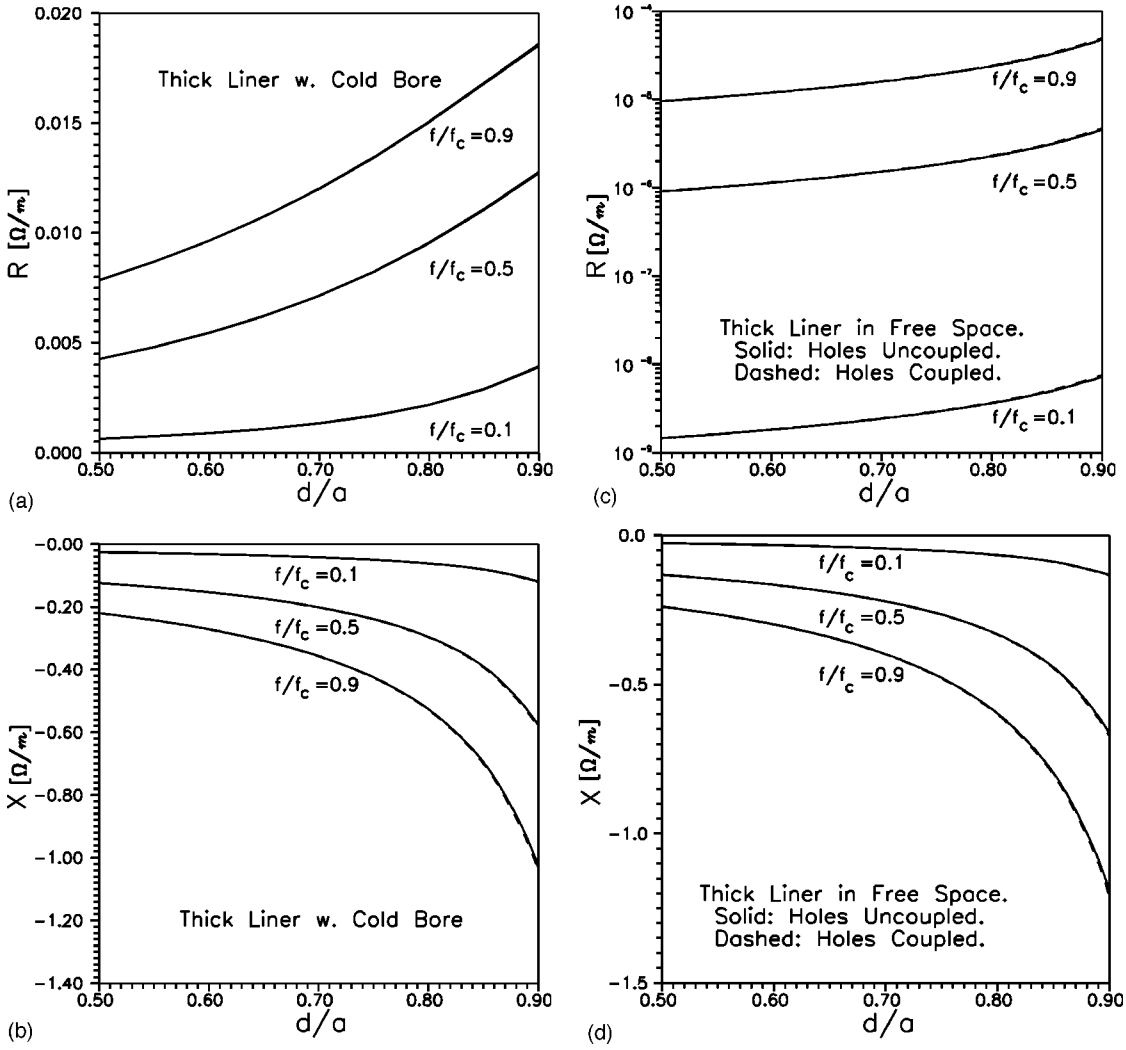

FIG. 4. (a) Rounded-corner square liner (see Fig. 3 and Table I). Thick liner with coaxial circular cold bore. Perforated wall resistance vs d/a at various values of f/f_c. (b) Rounded-corner square liner (see Fig. 3 and Table I). Thick liner with coaxial circular cold bore. Perforated wall reactance vs d/a at various values of f/f_c. (c) Rounded-corner square liner (see Fig. 3 and Table I). Thick liner in free space. Perforated wall resistance vs d/a at various values of f/f_c. (d) Rounded-corner square liner (see Fig. 3 and Table I). Thick liner in free space. Perforated wall reactance vs d/a at various values of f/f_c.

on the bunch length and the (local, spectral) impedances $Z_{\rm wall}^{\rm (Cu)}$, $Z_{\rm wall}^{\rm (ss)}$ of the stainless-steel and copper-plated surfaces and are [49]

$$W_{\rm ss,Cu}^{(0)}\left(\frac{\sigma_z}{a}\right)=2\int_0^{+\infty}e^{-(\sigma_z^2/a^2)(y^2/\beta_0^2)}{\rm Re}\left[Y_0 Z_{\rm wall}^{\rm (ss,Cu)}\left(\frac{yc}{a}\right)\right]dy, \tag{57}$$

where $y=\pi\omega/\omega_c$, $\omega_c=\pi c/a$ being the already defined cutoff frequency of the first waveguide mode in the (square) liner, and the wall impedances $Z_{\rm wall}^{\rm (ss,Cu)}$ refer to the unperforated (stainless-steel, copper) chamber walls. In Fig. 6 we plot $W_{\rm ss}^{(0)}(\sigma_z/a)$, using the parameters in Table I. The corresponding values of $W_{\rm Cu}^{(0)}(\sigma_z/a)$ are easily deduced since $W_{\rm ss}^{(0)}/W_{\rm Cu}^{(0)}=\sqrt{\rho_{\rm ss}/\rho_{\rm Cu}}\approx 30$.

B. Power loss through the holes

Here we discuss the most general case where holes are also drilled on the flat (copper-plated) portions of the liner wall. Accordingly, the power leaking through the holes, and dissipated in the stainless-steel inner and outer walls of the coaxial region, can be written as $P_{\rm Cu}^{\rm (holes)}+P_{\rm ss}^{\rm (holes)}$, where

$$P_{\rm Cu}^{\rm (holes)}=N_b\nu_r\frac{Q^2cZ_0}{8\pi^3a^2}W_{\rm Cu}^{\rm (holes)}\left(\frac{\sigma_z}{a}\right)G_{\rm Cu}\left(\frac{d}{a}\right), \tag{58}$$

$$P_{\rm ss}^{\rm (holes)}=N_b\nu_r\frac{Q^2cZ_0}{8\pi^3a^2}W_{\rm ss}^{\rm (holes)}\left(\frac{\sigma_z}{a}\right)G_{\rm ss}\left(\frac{d}{a}\right), \tag{59}$$

represent the contribution of the holes drilled on the stainless-steel (rounded corners) and copper-plated (straight sides) portions of the liner's wall. In Eqs. (58) and (59),

$$W_{\rm ss,Cu}^{\rm (holes)}\left(\frac{\sigma_z}{a}\right)=2\int_0^{+\infty}e^{-(\sigma_z^2/a^2)(y^2/\beta_0^2)}\times{\rm Re}\left[Y_0 Z_{\rm wall\ (ss,Cu)}^{\rm (holes)}\left(\frac{yc}{a}\right)\right]dy, \tag{60}$$

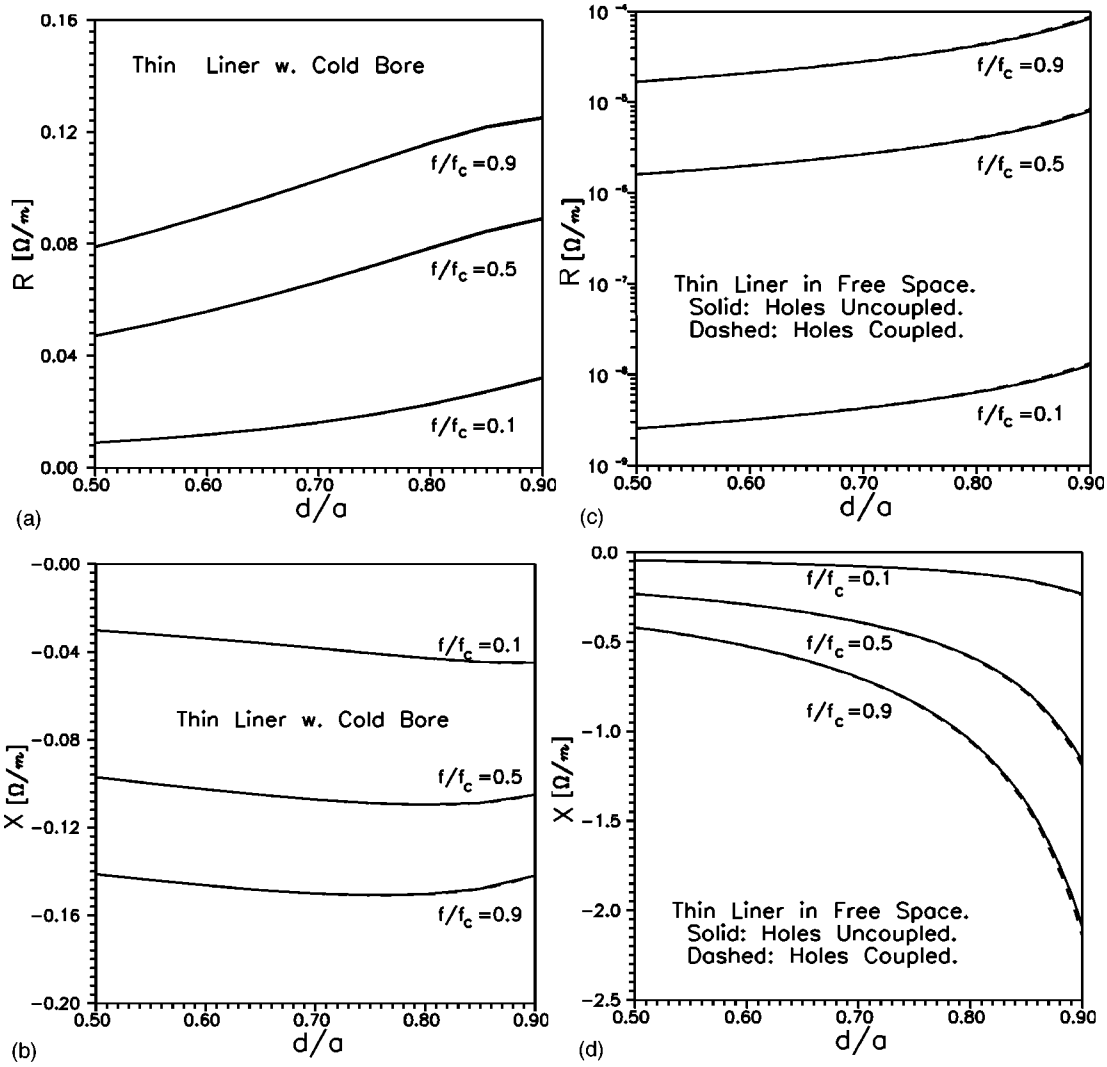

FIG. 5. (a) Rounded-corner square liner (see Fig. 3, Table I). Thin liner with coaxial circular cold bore. Perforated wall resistance vs d/a at various values of f/f_c. (b) Rounded-corner square liner (see Fig. 3 and Table I). Thin liner with coaxial circular cold bore. Perforated wall reactance vs d/a at various values of f/f_c. (c) Rounded-corner square linear (see Fig. 3 and Table I). Thin linear in free space. Perforated wall resistance vs d/a at various values of f/f_c. (d) Rounded-corner square liner (see Fig. 3 and Table I). Thin liner in free space. Perforated wall reactance vs d/a at various values of f/f_c.

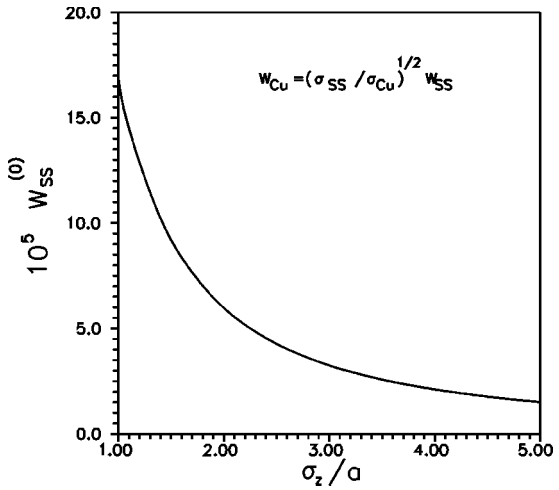

FIG. 6. The function $W_{ss}^{(0)}(\sigma_z/a)$ for the unperforated rounded-corner square liner (see Fig. 3).

where $Z_{\text{wall (ss,Cu)}}^{(\text{holes})}$ is the appropriate wall impedance (49), which depends on the number of holes per unit surface:

$$n_\sigma^{(\text{Cu})}=\frac{N_\lambda^{(\text{Cu})}}{4a}\left(\frac{d}{a}\right)^{-1}, \tag{61}$$

$$n_\sigma^{(\text{ss})}=\frac{N_\lambda^{(\text{ss})}}{4a}\left[\frac{\pi}{4}\left(1-\frac{d}{a}\right)\right]^{-1}, \tag{62}$$

$N_\lambda^{(\text{Cu,ss})}$ being the number of holes per unit length on the copper-plated and stainless-steel portions of the liner's wall.

The Ohmic power losses in the perforated pipe can be approximately written as

$$P_{\text{Cu,ss}}=(1-\alpha_{\text{Cu,ss}})P_{\text{Cu,ss}}^{(0)}, \tag{63}$$

where $P_{\text{Cu,ss}}^{(0)}$ are computed using Eqs. (56) and (57), and $\alpha_{\text{Cu,ss}}$ are the hole-covered copper and steel surface fractions, respectively.

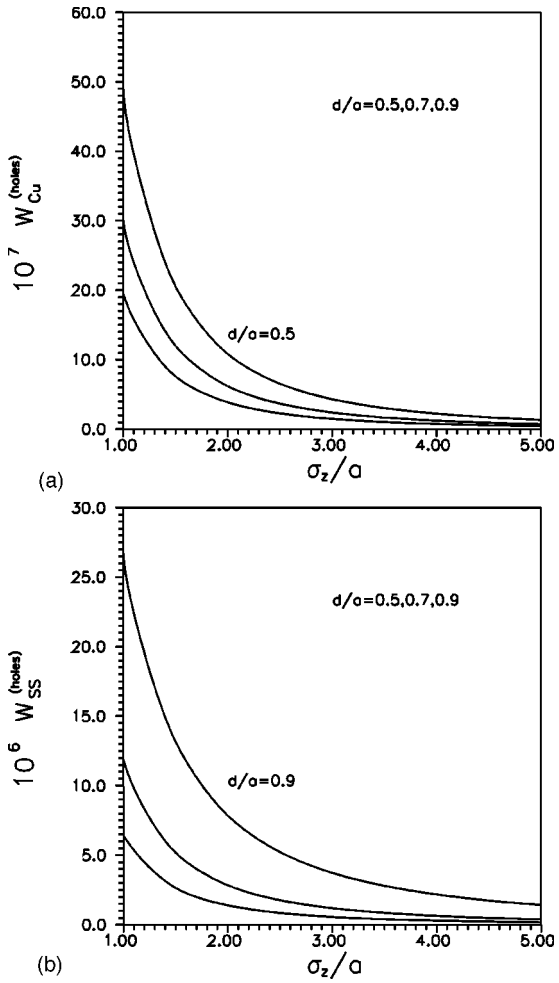

FIG. 7. (a) Rounded-corner square liner (see Fig. 3 and Table I). Holes confined to the straight sides. The function $W_{\mathrm{Cu}}^{(\mathrm{holes})}(\sigma_z/a)$ for several values of d/a. (b) Rounded-corner square liner (see Fig. 3 and Table I). Holes confined to the rounded corners. The function $W_{\mathrm{ss}}^{(\mathrm{holes})}(\sigma_z/a)$ for several values of d/a.

In order to check whether it is really more convenient to place the pumping holes on the rounded corners only, in the following we shall focus on the special cases where the pumping holes are *either* confined to the copper-plated strips (case I, $N_\lambda^{(\mathrm{ss})}=\alpha_{\mathrm{ss}}=P_{\mathrm{ss}}^{(\mathrm{holes})}=0$) *or* to the stainless-steel rounded corners (case II, $N_\lambda^{(\mathrm{Cu})}=\alpha_{\mathrm{Cu}}=P_{\mathrm{Cu}}^{(\mathrm{holes})}=0$) of the beam pipe.

In Figs. 7(a) and 7(b) we plot the functions $W_{\mathrm{ss,Cu}}^{\mathrm{holes}}(\sigma_z/a)$ for different values of d/a, for case I and case II, respectively [50], as functions of the ratio σ_z/a, assuming $N_\lambda=2660$ holes/m and circular holes of 1.5 mm diam (fixed pumping capacity).

As a result, we get the values summarized in Tables II and III.

In the limiting case where $d/a=0$ (all-steel circular chamber), we get $P_{\mathrm{ss}}^{(0)}\approx 2.06$ W/m, $P_{\mathrm{ss}}^{(\mathrm{holes})}\approx 14.4$ mW/m , whereas in the other limiting case $d/a=1$ (all-copper square chamber) we obtain [51] $P_{\mathrm{Cu}}^{(0)}\approx 68$ mW/m, $P_{\mathrm{Cu}}^{(\mathrm{holes})}\approx 10$ mW/m.

VIII. CONCLUSIONS

While relying on several simplifying assumptions (*perturbative* computation of beam coupling impedances and *approximate* boundary condition), the proposed approach includes in a remarkably simple fashion several nonobvious features which are not as easily included in the standard approach.

TABLE II. Parasitic losses. Case I: Holes confined to copper-plated straight sides in Fig. 3.

	$d/a=0.5$	$d/a=0.7$
P_{Cu}	54 mW/m	63 mW/m
P_{ss}	326 mW/m	72 mW/m
$P_{\mathrm{Cu}}^{(\mathrm{holes})}$	30 mW/m	19 mW/m
P_{total}	410 mW/m	154 mW/m

We suggest that the combined use of reciprocity formulas [Eqs. (1) and (2)] and impedance boundary conditions such as Eq. (36) provides a powerful tool to obtain analytical estimates of the beam coupling impedances in realistic, complex, and heterogeneous geometries.

As hints for future work, we mention (i) the possibility of deriving more accurate variational formulas for beam coupling impedances, (ii) the statistical characterization of the beam coupling impedances for randomly placed holes, (iii) the extension to ideally more accurate higher-order impedance boundary conditions, as discussed in [25,53–56], and finally (iv) the inclusion of pipe wall roughness.

APPENDIX A: IMPEDANCE BOUNDARY CONDITIONS

In this appendix we summarize a number of issues about impedance boundary conditions. No explicit derivations are provided, but pertinent references are given.

Impedance boundary conditions were introduced and extensively studied by the Russian School [53–57], and are usually credited to Leontóvich [10]. They relate the tangential electric and magnetic fields on the exterior boundary ∂V^- of a given domain V, thus allowing to solve an electromagnetic boundary value problem by solving Maxwell equations in the exterior domain only. In the simplest form, they are

$$\left|(\bar{\bar{I}}-\hat{u}_n\hat{u}_n)\cdot\vec{E}-Z_{\mathrm{wall}}\hat{u}_n\times\vec{H}\right|_{\partial V^-}=0, \tag{A1}$$

where Z_{wall} is the (local) characteristic impedance of the medium in V, and the fields are computed at ∂V^-.

These conditions can be applied at the surface ∂V of a *homogeneous*, isotropic body with refractive index n and smallest curvature radius or dimension R provided that [53–57]

TABLE III. Parasitic losses. Case II: Holes confined to stainless-steel rounded corners in Fig. 3.

	$d/a=0.5$	$d/a=0.7$
P_{Cu}	58 mW/m	66 mW/m
P_{ss}	298 mW/m	62 mW/m
$P_{\mathrm{ss}}^{(\mathrm{holes})}$	7.2 mW/m	3.3 mW/m
P_{total}	363 mW/m	131 mW/m

$$n \gg 1, \quad \mathrm{Im}(n) kR \gg 1. \tag{A2}$$

For an *open* surface ∂V (limiting a medium of infinite extent) for which *no* inward normal intersects the surface more than once, the second condition in Eq. (A2) can be relaxed into a milder one:

$$|n| kR \gg 1. \tag{A3}$$

For a *flat* open surface, the first condition in Eq. (A2) is sufficient. These equations admit simple physical interpretations.

For a plane open interface, the first of Eq. (A2) implies via Snell's law that the transmitted field is a plane wave, and Eq. (A1) follows from the continuity of the field components tangent to ∂V.

For nonplanar open interfaces, Eq. (A3) implies that the surface is planar at the level of the leading Fresnel zone [57], which makes Eq. (A1) asympotically valid in $(|n|kR)^{-1}$.

For a *compact* body, or an open but *reentrant* surface, the second equation in Eq. (A2) essentially ensures that the field penetration is much smaller than R, so that the waves are *not* transmitted beyond the body.

For *nonhomogeneous* bodies, it can be shown that [58]

$$|(\bar{\bar{I}} - \hat{u}_n \hat{u}_n) \cdot \vec{E} - Z_{\mathrm{wall}} \hat{u}_n \times \vec{H}|_{\partial V} = O\left(\frac{1}{kZ_0} \frac{\partial Z_{\mathrm{wall}}}{\partial n} \right) + O\left(\frac{1}{kZ_0} |\nabla_t Z_{\mathrm{wall}}| \right)^2 .$$

Equations (A1) therefore do apply *locally*, provided Z_{wall} is uniform over scales of the order of the wavelength in V. Higher-order boundary conditions have been introduced by several authors [26,58–61], For *locally* plane *stratified* media, simple transmission line formulas are sufficiently accurate for all practical purposes.

APPENDIX B: EFFECTIVE POLARIZABILITY IN A PLANE REGULAR HOLE ARRAY

In this appendix, for the reader's convenience we summarize the approach developed in [62–64] to compute the effective (electrical or magnetical) polarizability α' of a single hole (possibly noncircular) in a plane regular array. The induced dipole moment f is related to the pertinent field component by

$$\vec{f} = \alpha (\vec{F}_0 + \vec{F}_{\mathrm{int}}), \tag{B1}$$

where α is the polarizability of a single hole, $\vec{F}_0$ is the incident field, and $\vec{F}_{\mathrm{int}}$ is the *interaction* field acting on each hole due to the presence of all other holes. These latter are due to the very existence of the induced dipoles, and can thus be written as

$$\vec{F}_{\mathrm{int}} = C \vec{f}, \tag{B2}$$

where C depends only on the dipole orientation and the array geometry, *not* on the type of field (electric or magnetic).

According to Eqs. (B1) and (B2), the effective polarizability is given by

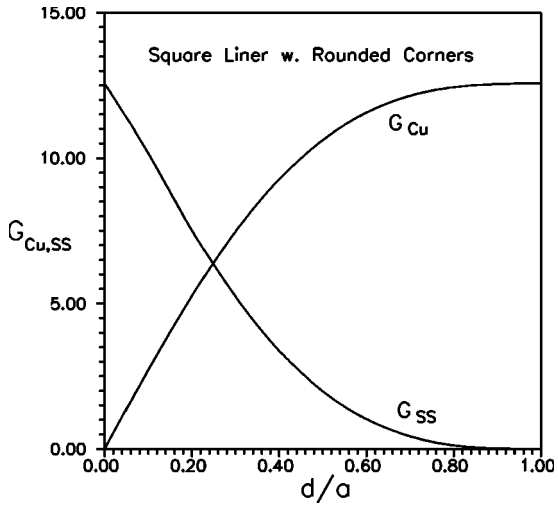

FIG. 8. The functions $G_{\mathrm{Cu,ss}}(d/a)$ for the rounded-corner square liner (see Fig. 3).

$$\alpha' = \frac{\alpha}{1 - \alpha C}. \tag{B3}$$

The interaction constant depends on the direction of the dipoles. It is convenient (superposition) to solve for the simplest cases where each induced dipole f is parallel to one of the coordinate axes. For the canonical problem sketched in Fig. 2, showing a plane regular array of y-directed dipoles placed at $\vec{r}_{nm} = (na_h)\vec{u}_x + (mb_h)\vec{u}_y$, the interaction constant will be denoted as C_y.

The general solution of this problem, which implies *no* restriction about the ratio between the dipole spacing and the wavelength, has been obtained by Collin ([64], problems 12.7 and 12.8). He also provides complete results for the simplest quasistatic case (hole spacing $\ll$ wavelength), appropriate for our present purposes, which are reported hereafter for the reader's convenience:

$$C_y = \frac{6}{5\pi b_h^3} - \frac{8\pi}{b_h^3} K_0\left(\frac{2\pi a_h}{b_h} \right). \tag{B4}$$

More or less obviously, if the induced dipoles were directed along the x direction, one should interchange a_h and b_h in Eq. (B4). Hence

$$C_x \approx \frac{6}{5\pi a_h^3} - \frac{8\pi}{a_h^3} K_0\left(\frac{2\pi b_h}{a_h} \right). \tag{B5}$$

Finally, for z-directed dipoles the interaction constant can be written as

$$C_z = -(C_y + C_x). \tag{B6}$$

APPENDIX C: THE FUNCTIONS $G_{\mathrm{Cu,ss}}(d/a)$

The general formula (1) can be applied to estimate the real part of the longitudinal impedance of the rounded-corner square cross-section liner sketched in Fig. 3, using the exact solution E_0 for the field produced by a relativistic unit-charge particle traveling along the axis of a perfectly con-

ducting square-section pipe reported in [49], yielding

$$\mathrm{Re}[Z_{\parallel}(\omega)]=\frac{\epsilon_0}{\beta_0 c Q^2}Y_0\oint_{\partial S}\mathrm{Re}[Z_{\mathrm{wall}}]|E_{0n}(\vec{r},0)|^2\,d\ell. \tag{C1}$$

For the geometry of Fig. 3, the pipe wall cross-section contour ∂S can be written as $\partial S_{\mathrm{ss}}+\partial S_{\mathrm{Cu}}$, the first term representing the stainless-steel rounded corners and the second one the copper-plated flat sides. Thus, Eq. (C1) can be further written as

$$\mathrm{Re}[Z_{||}(\omega)]=\frac{\mathrm{Re}[Z_{\mathrm{wall}}^{(\mathrm{ss})}]}{4\pi^2 a}G_{\mathrm{ss}}(d/a)+\frac{\mathrm{Re}[Z_{\mathrm{wall}}^{(\mathrm{Cu})}]}{4\pi^2 a}G_{\mathrm{Cu}}(d/a), \tag{C2}$$

where $Z_{\mathrm{wall}}^{(\mathrm{ss})}, Z_{\mathrm{wall}}^{(\mathrm{Cu})}$ are the wall impedances for the unperforated stainless-steel and copper-plated chamber walls, respectively, and

$$G_{\mathrm{Cu,ss}}=\oint_{\partial S_{\mathrm{Cu,ss}}}|\mathcal{E}_n(\vec{r},0)|^2\frac{d\ell}{a}, \tag{C3}$$

with

$$\vec{\mathcal{E}}(\vec{r},0)=(2\pi\epsilon_0 a)\vec{E}_0(\vec{r},0). \tag{C4}$$

The functions $G_{\mathrm{Cu,ss}}$ are shown in Fig. 8.

[1] The LHC Study Group, CERN/AC/95-05 (LHC), 1995 (unpublished).

[2] S.S. Kurennoy, CERN Report No. SL 91-29 (AP), 1991 (unpublished); Part. Accel. **39**, 1 (1992); and (unpublished).

[3] S.S. Kurennoy, IHEP 92-84; SSCL-636, 1993 (unpublished); Proc. EPAC, London, 1994 (unpublished); Part. Accel. **50**, 167 (1995).

[4] R.L. Gluckstern, CERN Report No. SL 92-05 (AP) (unpublished); CERN Report No. SL 92-18 (AP) (unpublished); Phys. Rev. A **46**, 1106 (1992).

[5] S.S. Kurennoy and R.L. Gluckstern (unpublished).

[6] S. Petracca, CERN/SL 99-03 (AP), 1999 (unpublished).

[7] S. De Santis *et al.* (unpublished); Phys. Rev. E **54**, 800 (1996).

[8] F. Caspers, E. Jensen, and F. Ruggiero, CERN/PS 92-24 (RF-AR) (unpublished); CERN/SL 92-15 (DI) (unpublished); LHC Note 186, 1992 (unpublished).

[9] F. Ruggiero, Part. Accel. **50**, 83 (1995).

[10] M.A. Leontóvich, *Issledovanya po Raspostraneniyu Radiovoln* (USSR Acad. Press, Moscow, 1948).

[11] Recently we became aware of some work by V. I. Bal'bekov (IHEP Report Nos. 93-55 to 93-57), where impedance boundary conditions were used to compute the longitudinal impedance of electrically small insertions.

[12] S. Petracca, Part. Accel. **50**, 211 (1995).

[13] The beam impedances are obviously independent of the total beam charge, as the fields in Eqs. (1) and (2) are proportional to Q.

[14] A.W. Chao, *Physics of Collective Beam Instabilities in High Energy Accelerators* (Wiley, New York, 1993), Sec. 2.4.

[15] A notable result of Kurennoy's analysis is related to the occurrence of *trapped modes* in the neighborhood of pipe discontinuities, including holes [16].

[16] G.V. Stupakov and S.S. Kurennoy, Phys. Rev. E **49**, 794 (1994).

[17] Kurennoy has also computed the (negligible, real) correction to Eq. (5) resulting from radiation leakage through the holes [3].

[18] H. Bethe, Phys. Rev. **66**, 163 (1944).

[19] The polarizabilities for a variety of hole shapes can be found in [20–22].

[20] S.B. Cohn, IRE Proc. **39**, 1416 (1952).

[21] F. de Meulenaere and J. van Bladel, IEEE Trans. Antennas Propag. **Ap-25**, 198 (1977).

[22] R. de Smedt and J. van Bladel, IEEE Trans. Antennas Propag. **AP-28**, 703 (1980).

[23] The only restrictive underlying assumption is that the holes should be (piecewise) uniformly distributed in the longitudinal direction, which is needed for the very definition of beam impedance per unit length to apply.

[24] S. S. Kurennoy (unpublished).

[25] T.B.A. Senior, IEEE Trans. Antennas Propag. **AP-29**, 826 (1981).

[26] Since we are interested in computing the hole-produced field in $z<0$, we use the so-called *internal* hole polarizabilities in Eq. (14).

[27] The field computed in this way fails to reproduce the *true* field for $z>0$. If one were interested in computing the fields in $z>0$, one should use the *external* polarizabilities in Eq. (14) before applying the image theorem. In this case, the computed field would not reproduce the true field for $z<0$.

[28] Compare with $\vec{k}^{(r)}$ in Eq. (12).

[29] In the asymptotic case of our interest, $\theta\to\pi/2$, all higher-order grating lobe waves $(p,q\neq 0)$ decay exponentially off the $z=0$ plane, as seen from Eq. (25).

[30] We remind the reader that the oblique wave impedance of a plane wave is defined as the ratio between the components of $\vec{E}$ and $\vec{H}$ transverse to the direction of propagation $\vec{k}$.

[31] The scattered specular magnetic field has only a nonzero y component.

[32] Note that in the limit of vanishingly small holes, we get $Z_{z>0}=0$ (perfect conductor), and hence we expect $|Z_{z>0}/Z_{z<0}|\ll 1$.

[33] J. Van Bladel, Radio Sci. **14**, 319 (1979).

[34] W.H. Cheng *et al.* (unpublished).

[35] A.V. Fedotov and R.L. Gluckstern, Phys. Rev. E **56**, 3583 (1997).

[36] N. McDonald, IEEE Trans. Microwave Theory Tech. **MTT-20**, 689 (1972).

[37] R.L. Gluckstern and J.A. Diamond, IEEE Trans. Microwave Theory Tech. **MTT-39**, 274 (1991).

[38] W.H. Cheng *et al.* (unpublished).

[39] B. Radak and R.L. Gluckstern, University of Maryland Report No. UMDP 93-112, 1993 (unpublished).

[40] W.H. Eggiman, IRE Trans. Microwave Theory Tech. **MTT-9**, 408 (1961).
[41] R.L. Gluckstern, CERN Report No. SL 92-06 (AP), 1992 (unpublished).
[42] R.L. Gluckstern, CERN Report No. SL 92-31 (AP), 1992 (unpublished).
[43] R.L. Gluckstern and B.W. Zotter, CERN Report No. SL 96-56 (AP), 1996 (unpublished).
[44] Equation (45) was first deduced by Gluckstern [41], although apparently neglecting the *complex* character of $\hat{\delta}$.
[45] This is a more or less obvious consequence of the r^{-1} dependence of the TEM fields in the coaxial region.
[46] The parasitic losses in the coaxial region have been computed in [8]. The result obtained in [8] using a different approach is recovered in the (appropriate) limit $|\alpha_e^{(i)}+\alpha_m^{(i)}| \ll |n_\sigma^{-1}\hat{\delta}(1+b/a)|$. Note that for a pointlike bunch $I(z,t)=Q\beta c\,\delta(z-\beta ct)$, one has $|F|=|I_{\rm cb}(z,\omega)/I(z,\omega)|$, where $I_{\rm cb}$ is the current in the coaxial transmission-line region between the pipe and the cold bore.
[47] Note that $s \geqslant 2r_0$, to keep holes separate.
[48] Below the (lowest) cutoff frequency, coupling among the holes will be essentially static, consistent with Eqs. (42) and (43). This can be understood by noting that, in the relativistic regime, the beam field is deducible from a (transverse, scalar) potential depending on $z-ct$, and that below cutoff no fields could propagate from one hole to another.
[49] S. Petracca, CERN Report No. SL 95-109 (AP), 1995 (unpublished).
[50] Note that for case I and case II, d/a must be, respectively, larger than $\pi^{-1}(S_h N_\lambda/4a)$ and smaller than $1-(4/\pi)^{-2}(S_h N_\lambda/4a)$, to prevent adjacent holes from merging, S_h being the single hole area.
[51] The quoted Ohmic losses are smaller than measured by a factor 2. This discrepancy is probably due to the roughness of the internal chamber wall [52].
[52] F. Caspers, M. Morvillo, and F. Ruggiero, CERN LHC Project Report No. 115 (1997) (unpublished); and unpublished.
[53] T.B.A. Senior, Rev. Sci. Instrum. B **8**, 419 (1960).
[54] S.M. Rytov, J. Exp. Theor. Phys. **10**, 120 (1940).
[55] V.A. Fock, J. Phys. (Moscow) **10**, 13 (1946).
[56] E.L. Feinberg, Nuovo Cimento Suppl. **11**, 60 (1959).
[57] We recall that the first Fresnel zone around a point is a circle centered at that point such that the distance of the observer from the center is $\lambda/2$ less than the distance from the rim.
[58] L.N. Trefethen and L. Halpern, Math. Comput. **47**, 421 (1986).
[59] J.L. Volakis and T.B.A. Senior, Proc. IEEE **77**, 5 (1989).
[60] M. Idemen, Proc. Phys. Soc. Jpn. **59**, 71 (1990).
[61] D.J. Hoppe and Y. Rahmat-Samii, J. Electromagn. Waves Appl. **8**, 1303 (1994).
[62] J. Brown and W. Jackson, Proc. IEEE **B102**, 37 (1955).
[63] H.S. Bennett, J. Appl. Phys. **24**, 785 (1953).
[64] R.E. Collin, *Field Theory of Guided Waves* (IEEE Press, Piscataway, NJ, 1991).